

## ARTICLE OPEN



# Scalable quantum computer with superconducting circuits in the ultrastrong coupling regime

Roberto Stassi<sup>1,2</sup>✉, Mauro Cirio<sup>3</sup> and Franco Nori<sup>1,4</sup>

So far, superconducting quantum computers have certain constraints on qubit connectivity, such as nearest-neighbor couplings. To overcome this limitation, we propose a scalable architecture to simultaneously connect several pairs of distant qubits via a dispersively coupled quantum bus. The building block of the bus is composed of orthogonal coplanar waveguide resonators connected through ancillary flux qubits working in the ultrastrong coupling regime. This regime activates virtual processes that boost the effective qubit–qubit interaction, which results in quantum gates on the nanosecond timescale. The interaction is switchable and preserves the coherence of the qubits.

npj Quantum Information (2020)6:67; <https://doi.org/10.1038/s41534-020-00294-x>

## INTRODUCTION

Superconducting circuits are a very promising hardware platform for quantum computers with capabilities beyond the ones of classical computers (see, e.g., refs. <sup>1–5</sup> and references therein). A basic requirement to perform quantum logic gates is to have controllable interactions among qubits (e.g., refs. <sup>6–9</sup>). Obviously, quantum computers benefit from higher and better connectivity among qubits, and this becomes more challenging to achieve as the system is scaled up. Unfortunately, so far, superconducting quantum computers have certain constraints on qubit connectivity, such as nearest-neighbor couplings<sup>10</sup>. Although the distant interaction between two or more qubits, mediated by a cavity bus, has been demonstrated (e.g., refs. <sup>11–13</sup>), this scheme is not convenient to connect many pairs of distant qubits simultaneously in a superconducting quantum computer. Indeed, in this case, the qubit–qubit interaction is activated by tuning qubit frequencies, leading to possible unwanted couplings and to a reduction of the coherence time of the qubits.

In addition to applications to quantum computing, superconducting circuits are a very versatile platform to investigate new quantum phenomena and to engineer quantum devices (e.g., refs. <sup>14–21</sup>). Note that the coupling between a superconducting artificial atom (e.g., refs. <sup>22–25</sup>) and a resonator can be a significant fraction of the bare atom and cavity energies (e.g., refs. <sup>26–31</sup>). In this ultrastrong coupling regime, the usual Jaynes–Cummings approximation breaks down and the counter-rotating terms must be taken into account<sup>32,33</sup>.

Here, we theoretically propose a scalable architecture to simultaneously couple pairs of distant superconducting qubits. The building block of this architecture is composed of three waveguides. Two of them ( $C_1$  and  $C_2$ ), see Fig. 1a, are directly connected to the qubits ( $q_a$  and  $q_b$ ) that form the computational basis, while a third ( $C_3$ ) is connected to the first two in a  $\Pi$ -shape form. At the intersection point, the interaction is mediated by ancillary flux qubits ( $f_1$  and  $f_2$ ) in the ultrastrong coupling regime. All components of the  $\Pi$ -connector are on resonance with each other. However, the two qubits,  $q_a$  and  $q_b$ , are detuned with respect to the eigenenergies of the bus. The last condition

guarantees that the coupling between qubits is mediated by virtual excitations, thereby not affecting their coherence. Moreover, the bus takes advantage of the counter-rotating terms activated by the ultrastrong coupling, enhancing the coupling between the qubits. This allows to perform fast two-qubit gates on nanosecond timescales. To achieve scalability, these building blocks can be arranged in an array, see Fig. 1b, so that every qubit is connected with each other. Couplings between qubits can be switched on and off by tuning the ancillary flux qubit frequencies on and off resonance with the waveguides. Importantly, this allows the qubits  $q_a$  and  $q_b$  to remain in their optimal working point, preserving their coherence times.

## RESULTS

The Hamiltonian describing the  $\Pi$ -connector in Fig. 1a is  $\hat{H} = \hat{H}_q + \hat{H}_\Pi + \hat{H}_{\text{int}}$ , where  $\hat{H}_q = \frac{1}{2} \sum_{i=a,b} \omega_{q_i} \hat{\sigma}_z^{(i)}$  represents both qubit  $q_a$  and  $q_b$  ( $\hbar = 1$ ),

$$\hat{H}_\Pi = \frac{1}{2} \sum_{i=1}^2 \omega_f \hat{\sigma}_z^{(i)} + \sum_{i=1}^3 \omega_c \hat{a}_{(i)}^\dagger \hat{a}_{(i)} + \sum_{i=1}^2 \lambda_s \hat{\sigma}_x^{(i)} (\hat{X}_1 + \hat{X}_3) \quad (1)$$

is the Hamiltonian of the ultrastrongly coupled quantum bus, and  $\hat{H}_{\text{int}} = \lambda (\hat{\sigma}_x^{(a)} \hat{X}_1 + \hat{\sigma}_x^{(b)} \hat{X}_2)$  represents the interaction between the qubits and the quantum bus. Here,  $\hat{\sigma}_z^{(i)}$  and  $\hat{\sigma}_x^{(i)}$  are Pauli operators for the qubits  $q_a$  and  $q_b$  ( $i = a, b$ ) and for the flux qubits ( $i = 1, 2$ ), with transition energies  $\omega_{q_i} = \omega_q$  and  $\omega_{f_i} = \omega_c$ , respectively. We set the fundamental frequency of all resonators  $C_k$  to be  $\omega_c = 3\omega_q$ , and we denote the annihilation, creation, and quadrature operators by  $\hat{a}_{(k)}$ ,  $\hat{a}_{(k)}^\dagger$ , and  $\hat{X}_k = \hat{a}_{(k)} + \hat{a}_{(k)}^\dagger$  ( $k = 1, 2, 3$ ). Flux qubit  $f_1$  ( $f_2$ ) is ultrastrongly coupled to cavity  $C_1$  ( $C_2$ ) and  $C_3$ , with coupling strength  $\lambda_s > 0.1\omega_c$ . Instead, the coupling strength between qubit  $q_a$  ( $q_b$ ) and resonator  $C_1$  ( $C_2$ ) is set to  $\lambda = 0.05\omega_q$ . The latter interaction, operating in the dispersive regime, causes a shift in the qubit frequency,

$$\tilde{\omega}_{q_i} = \omega_{q_i} - \lambda^2 / (\omega_c + \omega_{q_i}), \quad (2)$$

and a dressing in the qubit states<sup>34,35</sup>. These qubit dressed states  $\{|0\rangle, |1\rangle\}$  are the ones forming our computational basis. We call

<sup>1</sup>Theoretical Quantum Physics Laboratory, RIKEN Cluster for Pioneering Research, Wako-shi, Saitama 351-0198, Japan. <sup>2</sup>Dipartimento di Scienze Matematiche e Informatiche, Scienze Fisiche e Scienze della Terra, Università di Messina, 98166 Messina, Italy. <sup>3</sup>Graduate School of China Academy of Engineering Physics, Haidian District 100193 Beijing, China. <sup>4</sup>Physics Department, The University of Michigan, Ann Arbor, MI 48109-1040, USA. ✉email: roberto.stassi@riken.jp

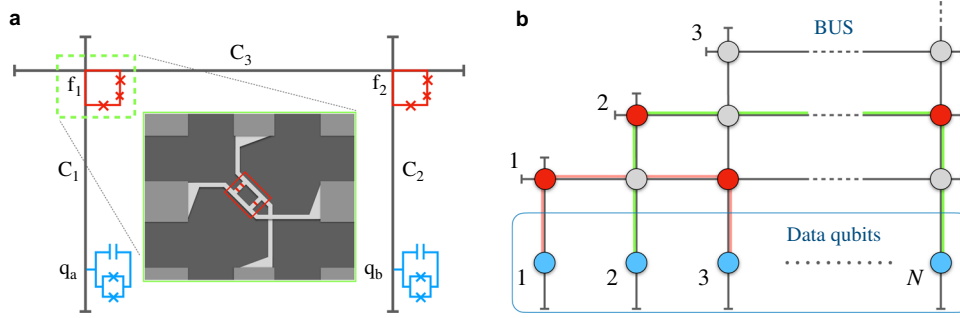


**Fig. 1**  **$\Pi$ -connector and scalable architecture.** **a** Sketch of the  $\Pi$ -connector. Dark gray lines represent the coplanar waveguide resonators,  $C_1$ ,  $C_2$ , and  $C_3$ . Red lines represent the flux qubits,  $f_1$  and  $f_2$ , connecting the waveguides. Blue lines represent the data qubits (transmon here, but could also be other types),  $q_a$  and  $q_b$ . The inset inside the green dashed square represents the connection between the flux qubit (red box) and the constriction of the center conductor of the two orthogonal waveguides (light gray). **b** An array of data qubits (blue disks) at the bottom part are connected through a net of waveguides. At each node, a flux qubit tuned with the waveguides (red disk) mediates the interaction between data qubits. The gray disks (connector is “OFF”) denote detuned flux qubits.

“data qubits” the dressed qubits, which are generating the computational basis.

The quantum bus provides an effective  $XX$  interaction between data qubits mediated by virtual excitations, as it is guaranteed by the detuning condition  $\omega_c - \omega_q = 2\omega_q$ . This interaction causes a two-qubit oscillation between states with one excitation:  $|1, 0\rangle$  and  $|0, 1\rangle$ . The inset of Fig. 2a shows the swap from the state  $|1, 0\rangle$  to the state  $|0, 1\rangle$  in a time  $t = \pi/\omega_R$ , where  $\omega_R = 2\lambda_{\text{eff}}$ , and  $\lambda_{\text{eff}}$  is the effective coupling strength between data qubits. At  $t = \pi/2\omega_R$ , as indicated by the arrow, a maximally entangled Bell state is generated, and a universal  $\sqrt{i}$ SWAP gate is obtained. Figure 2a shows the average gate fidelity<sup>36,37</sup>

$$\mathcal{F} = \int d\psi \langle \psi | \hat{U}_{\sqrt{i}\text{SWAP}}^\dagger \hat{\rho}_{|\psi\rangle} \hat{U}_{\sqrt{i}\text{SWAP}} | \psi \rangle \quad (3)$$

generated by the quantum bus as a function of the ultrastrong coupling  $\lambda_s$  (blue circles), taking into consideration decoherence channels originating from the components of the bus. Here,  $\hat{\rho}_{|\psi\rangle}$  is the resulting density matrix after evolving the system for a time  $t_{\sqrt{i}\text{SWAP}} = \pi/2\omega_R$ , under the action of the full Hamiltonian in Eq. (1). The integral in Eq. (3) uses the unitarily invariant measure  $d\psi$  on the state space, normalized such that  $\int d\psi = 1$ , the operator  $\hat{U}_{\sqrt{i}\text{SWAP}}$  is the ideal  $\sqrt{i}$ SWAP gate, and  $|\psi\rangle$  is the input state. For the data qubits, we choose  $T_1 = 70 \mu\text{s}$  and pure dephasing time  $T_\phi = 92 \mu\text{s}$  (data are taken from ref. <sup>35</sup>, which fulfill our parameter conditions).

When the interaction is activated, the ultrastrong coupling induces a small energy shift of the data qubit, resulting in a  $z$ -axis single-qubit rotation. This can be compensated using standard procedures<sup>38</sup>. In our simulations, it is compensated by a rotation in the opposite direction. Figure 2a also shows the average fidelity of the  $\sqrt{i}$ SWAP gate (red solid curve) when the data qubits are directly coupled through the ideal interaction Hamiltonian  $\lambda_{\text{eff}} \hat{\sigma}_x^{(a)} \hat{\sigma}_x^{(b)}$ . A comparison between the two curves proves that the bus does not affect the coherence of the data qubits, and shows that the only limitation to performance is the intrinsic decoherence of the data qubits. Considering data qubits with transition frequency of 4 GHz<sup>35</sup>, for  $\lambda_s = 0.32\omega_c$ , the fidelity is 99.87% and the gate time is 11.7 ns. Beyond this coupling point, the gate performance degrades due to the hybridization between the computational and bus states. All the dynamics are calculated using the master equation developed in ref. <sup>20</sup>, for  $T = 0$ .

Every type of superconducting qubit can be used as data qubit in our protocol. Currently, due to their long coherence time<sup>35</sup>, transmon qubits are commonly used. However, the low anharmonicity of these artificial atoms could lead to non-negligible detrimental effects on the gate performance. To estimate these

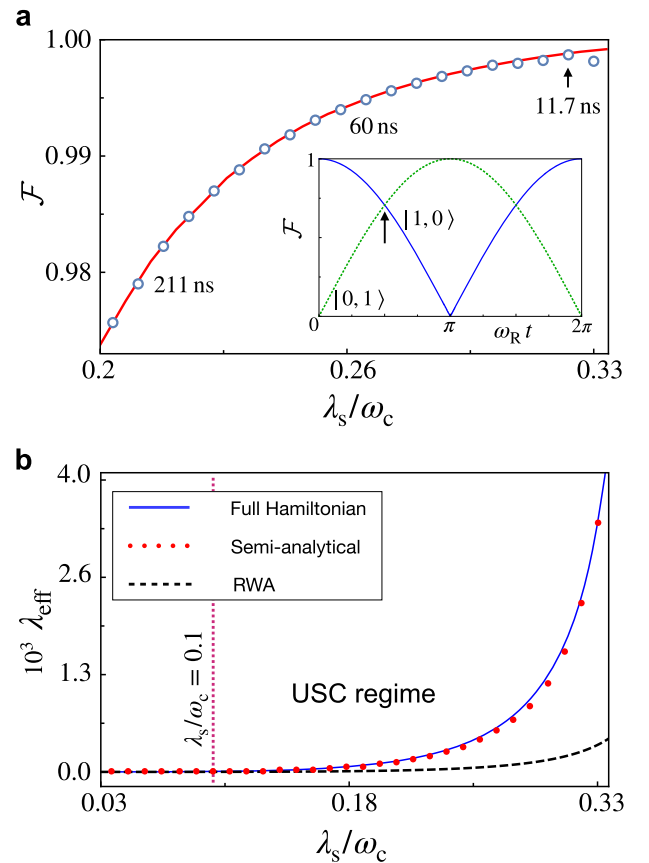


**Fig. 2** **Fidelity and effective coupling.** **a** Average gate fidelity of the  $\sqrt{i}$ SWAP gate generated by the quantum bus (blue circles) and by a direct qubit–qubit coupling (red solid curve) with coupling strength  $\lambda_{\text{eff}}$ . The chosen frequency transitions of the data qubits is  $\omega_q = 4$  GHz, the relaxation time is  $70 \mu\text{s}$  and the pure dephasing time is  $92 \mu\text{s}$ . Flux qubits have a relaxation time of  $20 \mu\text{s}$  and pure dephasing time of  $10 \mu\text{s}$ ; resonators have a  $Q$ -factor of  $5 \times 10^5$ . The inset shows the fidelity of the  $|1, 0\rangle$  (blue solid curve) and  $|0, 1\rangle$  states (green dotted curve). Here, the evolution is numerically calculated using the quantum bus, no dissipation is considered. **b** Effective coupling calculated numerically using the full Hamiltonian  $\hat{H}$  (solid blue curve), dropping the counter-rotating terms (dashed black curve) and calculated using the semi-analytical expression in Eq. (4) (red dots).

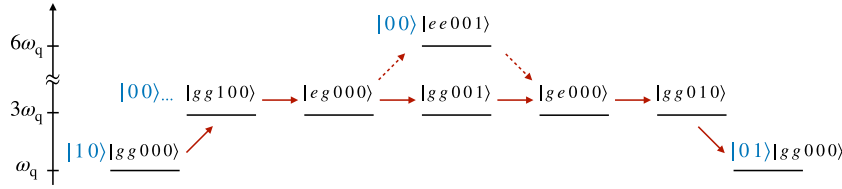


**Fig. 3 Virtual states connecting  $q_a$  and  $q_b$ .** The main path (solid arrows) connecting the states  $|1, 0\rangle$  and  $|0, 1\rangle$  (blue states) through the virtual bus states (black states). The order of the labels in the black kets is  $|f_1, f_2, C_1, C_2, C_3\rangle$ . The dashed arrows indicate a path due to the counter-rotating terms.

effects, we calculated the average gate fidelity using as data qubit the two lowest states of a three-level system with low anharmonicity. We set the transition frequency between the first and second excited states to  $0.8\omega_q$ , where  $\omega_q$  is now the transition frequency between the ground and the first excited state. All other parameters are as above. In this setting, the average gate fidelity is 99.72% for  $\lambda_s/\omega_c = 0.3$  (instead of 99.75% calculated using the two-level system). Moreover, in the absence of decoherence channels, the fidelity is 99.99%. These results indicate that the low anharmonicity has a negligible impact on the performance of the gate.

#### Effective coupling

As explained in the “Methods” section, to calculate the effective qubit–qubit coupling we perform a projection of the full Hamiltonian  $\hat{H}$  into the ground state of the bus Hamiltonian  $\hat{H}_\Pi$ . Considering the dispersive regime between data qubits and the bus, neglecting the dressing, the effective coupling becomes

$$\lambda_{\text{eff}} = \sum_k \frac{g_k^{(1)} g_k^{(2)}}{\omega_q - \Delta E_k}, \quad (4)$$

where  $E_k$  and  $|\tilde{k}\rangle$  are the eigenenergies and eigenstates of  $H_\Pi$ , and where  $g_k^{(i)} = \lambda \langle \tilde{k} | \hat{X}_i | \tilde{0} \rangle$  ( $i = 1, 2$ ), and  $\Delta E_k = E_k - E_0$ <sup>39</sup>. In Fig. 2b, we numerically computed the effective coupling as a function of  $\lambda_s$  using the full Hamiltonian  $\hat{H}$ , and compared it with Eq. (4). The agreement is very good in the coupling range under investigation. According to perturbation theory to sixth order<sup>40–42</sup>, the virtual processes that provide the main contribution to the qubit–qubit effective interaction, neglecting the dressing, are the ones that connect the state  $|1, 0\rangle|0\rangle_b$  to  $|0, 1\rangle|0\rangle_b$  (where  $|0\rangle_b = |g, g, 0, 0, 0\rangle$ ) through states with the lowest-energy differences with the initial state,  $|1, 0\rangle|0\rangle_b$ . It appears clear now that the main process, Fig. 3 (red solid arrows), is the one that transfers one excitation through all the elements that compose the bus. In the same diagram, it is also shown a virtual process (red dashed arrows) involving the simultaneous excitation of the flux qubit  $f_1$  and the resonator  $C_3$ , which is activated by the counter-rotating terms in the interacting part of the bus Hamiltonian  $\hat{H}_\Pi$ .

In the ultrastrong coupling regime, the counter-rotating terms become relevant and activate virtual processes that strongly boost the effective coupling. To prove this, we have numerically calculated the effective coupling after dropping the counter-rotating terms in  $\hat{H}$  (see Fig. 2b, dashed curve). Comparing this with the results from the full Hamiltonian (blue solid curve), we notice that  $\lambda_{\text{eff}}(\lambda_s)$ , calculated with the counter-rotating terms, increases much faster compared to the one calculated without it, as a function of the coupling  $\lambda_s$ . It is standard procedure in perturbation theory to use virtual excitations to derive an effective interaction. These are the virtual photons we are referring to, not the ones in the ultrastrong coupling of cavity QED.

#### Switch-on and switch-off of the effective interaction

To realize a properly scalable system, it is important to be able to switch-on and switch-off the interaction between arbitrary data qubits. We achieve this by tuning (switch-on) and detuning (switch-off) to the bus the transition frequency of the ancillary flux qubit by varying the external flux  $\Phi_{\text{ext}} = f\Phi_0$  threading it<sup>21</sup>. We set the switch-on condition at the optimal bias point,  $f \rightarrow f_{\text{on}} = 0.5$ , where the flux qubit has a symmetric potential energy and maximum dipole moment  $M_{\text{on}}$ <sup>43</sup>. To switch-off the interaction, we move the flux qubit away from its optimal point, by changing the external flux,  $f \rightarrow f_{\text{off}}$ .

If we detune  $f_1$  and  $f_2$  from the  $\Pi$ -connector in Fig. 1a, using  $f_{\text{off}} = 0.522$ , the flux qubit transition frequency becomes  $\approx 14 \omega_{f_1}$ , and the dipole moment becomes  $M_{\text{off}} = 6 \times 10^{-2} M_{\text{on}}$  (other parameters are provided in “Methods”). For  $\lambda_s = 0.3\omega_c$ , the residual interaction is  $\lambda_{\text{eff}}^{(\text{off})} \approx 2 \times 10^{-11} \omega_q$  and the on/off coupling ratio between data qubits is  $\approx 6 \times 10^7$ , which is almost independent of  $\lambda_s$ . When the flux qubit  $f_2$  is detuned and  $f_1$  is tuned, the on/off coupling ratio is  $\approx 9 \times 10^3$ . In this case, if the system consists of only two data qubits, no interaction occurs. This happens as the ultrastrong coupling shifts the frequency of data qubit  $q_a$  by a quantity larger than the residual effective coupling. For instance, if  $f_2$  is detuned and  $\lambda_s = 0.3\omega_c$ , the qubit  $q_b$  interacts with qubit  $q_a$  at  $\omega_{q_b} = \omega_q - 9.3 \times 10^{-4} \omega_q$ , with a residual effective coupling of  $\tilde{\lambda}_{\text{eff}}^{(\text{off})} = 1.5 \times 10^{-7} \omega_q$ . Note that when the flux qubits are not in the optimal bias point, a charge interaction with the second quadrature of the resonators is activated, but its contribution is negligible<sup>26</sup>.

#### Scalable architecture

Figure 1b shows a possible scalable architecture for quantum computation using the  $\Pi$ -connector. In the bottom part of Fig. 1b, we represent an array of data qubits (blue disks). In the upper part we present the quantum bus. At each node, ancillary flux qubits can either couple (red disks) or decouple (gray disks) to the waveguides, depending on their frequency. In this way, it is possible to control the connectivity among arbitrary pairs of data qubits. For example, in Fig. 1b qubit 1 is connected to qubit 3, and qubit 2 is connected to qubit  $N$ . It is also possible to connect more than two qubits simultaneously. If the fundamental mode of the superconducting coplanar resonator is 12 GHz<sup>35</sup>, and if the distance between two consecutive flux qubits in the resonator is 0.1 mm (which could be even shorter), it could be possible to connect about 100 data qubits. The effective interaction among  $N$  data qubits in the scalable architecture is described by

$$\hat{H}_I = \sum_{k=1}^{N-1} \sum_{l=k+1}^N k \lambda_{\text{eff}}^{kl} \hat{\sigma}_x^{(l)} \hat{\sigma}_x^{(k)}. \quad (5)$$

This considers that qubit 1 is connected (on or off) with all the other qubits using one path, qubit 2 is connected with the rest of the qubits using two paths for each qubit, qubit 3 is

connected with the remaining qubits using three paths, and so on.

To evaluate cross-talk, we calculate the interaction of qubit  $N$ , the one with more connections, with all the other data qubits in the off coupling condition,  $\lambda_{\text{eff}}^{kl} = \lambda_{\text{eff}}^{(off)}$ . From Eq. (5), we find

$$\hat{H}_1^{(N)} = \hat{\sigma}_x^{(N)} \left[ (N-1) \lambda_{\text{eff}}^{(off)} \hat{\sigma}_x^{(N-1)} + (N-2) \lambda_{\text{eff}}^{(off)} \hat{\sigma}_x^{(N-2)} + \dots + \lambda_{\text{eff}}^{(off)} \hat{\sigma}_x^{(1)} \right]. \quad (6)$$

Considering the  $(N-1)$  data qubits as a single effective qubit, which is interacting with qubit  $N$ ,  $\hat{\sigma}_x^{(k)} \rightarrow \hat{\sigma}_x$  for all  $k \neq N$ , we obtain

$$\hat{H}_1^{(N)} = \frac{N(N-1)}{2} \lambda_{\text{eff}}^{(off)} \hat{\sigma}_x^{(N)} \hat{\sigma}_x. \quad (7)$$

Now,

$$\Lambda_{\text{eff}}^{(off)} = \lambda_{\text{eff}}^{(off)} N(N-1)/2 \quad (8)$$

is the residual interaction that affects qubit  $N$  in the off coupling condition. For  $\lambda_s = 0.3\omega_c$ , using  $N = 100$  data qubits, the coupler has a numerically measured on/off ratio of  $\approx 12,000$ .

In this architecture, when each pair of data qubits is interacting, all the data qubits have the same frequency shift and the residual coupling  $\tilde{\lambda}_{\text{eff}}^{(off)}$  is active. It is possible to cancel out this small interaction by detuning every pair of interacting data qubits from all other pairs by a quantity larger than the residual interaction. This can be achieved by changing the flux qubit frequency, which in turn changes the data qubit dressing.

## DISCUSSION

By taking advantage of the large coupling between flux qubits and the modes of waveguides or LC resonators, we proposed a scalable architecture that allows to control the coupling between many distant qubits. We numerically showed that the effective coupling is boosted by the counter-rotating terms of the Rabi Hamiltonian, whose contribution become more relevant in the ultrastrong coupling regime. The switch-on and switch-off of the interaction between data qubits is controlled by the magnetic fluxes threading the flux qubits, which tune their transition frequencies to the bus. Note that the resonant condition among the waveguides and flux qubits in the bus does not have to be perfect, because there is considerable tolerance. In fact, the strength of the effective coupling does not depend on this condition, but it depends on the detuning between each element of the bus and the data qubits, and on the couplings between elements of the bus. However, the resonant condition between data qubits must be satisfied. Unfortunately, current fabrication tolerances do not allow to set the frequency of the qubits precisely, and SQUID loops must be used to tune the data qubit frequencies. However, near-future improvements in the fabrication quality of qubits will eventually allow to take full advantage of this proposal. We believe that this architecture might lead to a new generation of quantum computer architectures controlled by elements largely detuned from the data ones, allowing to increase the complexity of the system without affecting the coherence times. A natural evolution could be the connection of a matrix of data qubits through waveguides in a 3D circuit<sup>19</sup>.

## METHODS

### Effective coupling

In this section, we derive an effective model to describe the dynamics of two data qubits in contact with a quantum bus. We do this by projecting the full dynamics (which takes place in the total Hilbert space  $\mathcal{H}$  of both data qubits and bus) into the subspace  $\mathcal{H}_{\text{eff}} = P\mathcal{H}$ , where the bus is in the ground state. Here,  $\hat{P} = \hat{\mathbb{I}}_q \otimes |\bar{0}\rangle\langle\bar{0}|$  denotes the projector into the

ground state  $|\bar{0}\rangle$  of the bus ( $\hat{\mathbb{I}}_q$  being the identity operator on the data qubits).

As a first step, we decompose the total Hamiltonian  $\hat{H}$  into a “diagonal” contribution  $\hat{H}_0$  (which preserves  $\mathcal{H}_{\text{eff}}$ , i.e.,  $[\hat{H}_0, \hat{P}] = 0$ ) and an “off-diagonal” contribution  $\hat{V}$  (for which  $[\hat{V}, \hat{P}] \neq 0$ ). By defining a complementary projector  $\hat{Q}$ , such that  $\hat{P} + \hat{Q} = \hat{\mathbb{I}}$ , we can write

$$\begin{aligned} \hat{H} &= (\hat{P} + \hat{Q})\hat{H}(\hat{P} + \hat{Q}) \\ &= \hat{H}_0 + \hat{V}, \end{aligned} \quad (9)$$

where  $\hat{H}_0 = \hat{P}\hat{H}\hat{P} + \hat{Q}\hat{H}\hat{Q}$  and  $\hat{V} = \hat{P}\hat{H}_{\text{int}}\hat{Q} + \hat{Q}\hat{H}_{\text{int}}\hat{P}$ . The potential  $\hat{V}$  can be explicitly written as

$$\begin{aligned} \hat{V} &= \sum_k \left[ g_k^{(1)} \hat{\sigma}_x^{(a)} \left( |\bar{k}\rangle\langle\bar{0}| + |\bar{0}\rangle\langle\bar{k}| \right) + g_k^{(2)} \hat{\sigma}_x^{(b)} \left( |\bar{k}\rangle\langle\bar{0}| + |\bar{0}\rangle\langle\bar{k}| \right) \right] \\ &\simeq \sum_k \left[ g_k^{(1)} \hat{\sigma}_x^{(a)} |\bar{k}\rangle\langle\bar{0}| + g_k^{(2)} \hat{\sigma}_x^{(b)} |\bar{k}\rangle\langle\bar{0}| \right] + \text{H.c.}, \end{aligned} \quad (10)$$

where we made a rotating-wave approximation under the assumption that  $|g_k^{(1)}|, |g_k^{(2)}| \ll \omega_q, \Delta E_k$ . We further assume to be in a dispersive regime, where the detuning between the splitting of the data qubits  $\omega_q$  and the transition energies of the bus  $\Delta E_k$  are much larger than the couplings  $g_k^{(1)}$  and  $g_k^{(2)}$  (i.e.,  $|\omega_q - \Delta E_k| \gg |g_k^{(1)}|, |g_k^{(2)}|$ ). In this limit, it is possible to perturbatively define a rotating frame where the dynamics is effectively constrained in  $\mathcal{H}_{\text{eff}}$  (Schrieffer–Wolff transformation). Specifically, a change of frame  $\exp[\hat{S}]$  (for an anti-Hermitian operator  $\hat{S}$ , such that  $[\hat{H}_0, \hat{S}] = \hat{V}$ ) allows to define the effective Hamiltonian

$$\hat{H}_{\text{eff}} = \hat{P}e^{\hat{S}}\hat{H}e^{-\hat{S}}\hat{P} \simeq \hat{P}\hat{H}_0\hat{P} + \frac{1}{2}\hat{P}[\hat{S}, \hat{V}]\hat{P}, \quad (11)$$

at the lowest nontrivial order in  $\hat{S}$ . Specifically, by choosing

$$\hat{S} = \sum_{k>0} \left( \frac{g_k^{(1)}}{\omega_q - \Delta E_k} \hat{\sigma}_+^{(a)} + \frac{g_k^{(2)}}{\omega_q - \Delta E_k} \hat{\sigma}_+^{(b)} \right) |\bar{0}\rangle\langle\bar{k}| - \text{H.c.}, \quad (12)$$

and computing the commutator  $[\hat{S}, \hat{V}]$  in Eq. (11), we obtain the effective coupling between the data qubits described in the main text.

### Flux qubit resonator

The energies and electric dipole moments were calculated considering a flux qubit composed of three Josephson junctions with energies  $E_{J1} = E_{J2} = E_J$ , and  $E_{J3} = \alpha E_J$ . The Hamiltonian of the flux qubit is<sup>43</sup>

$$H_F = E_C P_+ + \frac{E_C}{1+2\alpha} P_- + U(\varphi_+, \varphi_-), \quad (13)$$

with  $U(\varphi_+, \varphi_-) = -E_J[2 \cos \varphi_+ \cos \varphi_- + \alpha \cos(2\pi f + 2\varphi_+)]$ , having defined  $\varphi_+ = (\varphi_1 + \varphi_2)/2$  and  $\varphi_- = (\varphi_1 - \varphi_2)/2$ , where  $\varphi_1$  and  $\varphi_2$  are the phase drops across the larger junctions.  $P_+$  and  $P_-$  are the conjugate momenta of  $\varphi_+$  and  $\varphi_-$ . Choosing  $E_J = 35E_C$ ,  $E_C = 27.1$  GHz, and  $\alpha = 0.8$ , the dipole moment was determined by the matrix element  $\langle g | \sin(2\pi f + 2\varphi_+) | e \rangle$ .

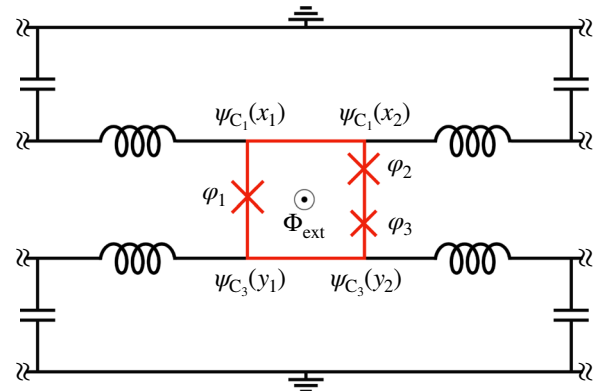


**Fig. 4 Equivalent circuit diagram.** Coplanar waveguides (black lines) connected to the flux qubit (red lines).

## Interaction between a flux qubit and two orthogonal coplanar waveguides

The derivation of the flux qubit-resonator Hamiltonian  $\hat{H}_\Pi$  is standard<sup>26</sup>, but here the voltage condition for the flux qubit (red loop in Fig. 4) is  $\sum_{i=1}^3 \varphi_i + \Delta\psi_{C_1} + \Delta\psi_{C_2} = \Phi_{\text{ext}}$ , where  $\Delta\psi_{C_1} = \psi_{C_1}(x_2) - \psi_{C_1}(x_1)$  and  $\Delta\psi_{C_2} = \psi_{C_2}(y_1) - \psi_{C_2}(y_2)$ .

The ultrastrong coupling between a flux qubit and two superconducting coplanar stripline resonators has been experimentally realized<sup>44</sup>. However, our scheme further requires the waveguides to cross and the resonator modes not to be significantly modified by the coupling with the flux qubit. The inset in Fig. 1a represents a sketch of the connection between the orthogonal waveguides mediated by the ancillary flux qubit. The latter is directly connected to both the center conductor of the coplanar waveguide transmission-line resonators, see also Fig. 4. At the insertion point, the width of the center conductor is narrower and the local inductance is larger, to enhance the coupling between the flux qubit and the resonator<sup>26</sup>. The three Josephson junctions forming the flux qubits must be inserted in the two tiny flux qubit arms that connect the center conductors of both waveguides. In this way, the current in the resonator flows predominantly through the center conductor constrictions of the waveguides and the resonator modes are not significantly modified. Since the distribution of the electromagnetic field is not uniform in the resonator, we suggest to fabricate waveguides with progressively narrower constrictions, in order to maintain a uniform coupling for all qubits. Alternatively, one can increase the coupling strength by inserting several Josephson junctions in the constrictions with a progressively increasing inductance along the waveguide<sup>26</sup>.

## DATA AVAILABILITY

Data are available from the corresponding author on reasonable request.

Received: 26 February 2019; Accepted: 16 June 2020;

Published online: 06 August 2020

## REFERENCES

- Barends, R. et al. Superconducting quantum circuits at the surface code threshold for fault tolerance. *Nature* **508**, 500–503 (2014).
- Mohseni, M. et al. Commercialize quantum technologies in five years. *Nature* **543**, 171–174 (2017).
- IBM. The quantum experience. <https://www.research.ibm.com/quantum/> (2016).
- Boixo, S. et al. Characterizing quantum supremacy in near-term devices. *Nat. Phys.* **14**, 595–600 (2018).
- Arute, F. et al. Quantum supremacy using a programmable superconducting processor. *Nature* **574**, 505–510 (2019).
- Grajcar, M. et al. Switchable resonant coupling of flux qubits. *Phys. Rev. B* **74**, 172505 (2006).
- Liu, Y.-x et al. Controllable coupling between flux qubits. *Phys. Rev. Lett.* **96**, 067003 (2006).
- Plantenberg, J. H. et al. Demonstration of controlled-NOT quantum gates on a pair of superconducting quantum bits. *Nature* **447**, 836–839 (2007).
- Ashhab, S. et al. Interqubit coupling mediated by a high-excitation-energy quantum object. *Phys. Rev. B* **77**, 014510 (2008).
- Linke, N. M. et al. Experimental comparison of two quantum computing architectures. *Proc. Natl Acad. Sci. USA* **114**, 3305–3310 (2017).
- DiCarlo, L. et al. Demonstration of two-qubit algorithms with a superconducting quantum processor. *Nature* **460**, 240–244 (2009).
- DiCarlo, L. et al. Preparation and measurement of three-qubit entanglement in a superconducting circuit. *Nature* **467**, 574 (2010).
- Song, C. et al. Generation of multicomponent atomic Schrödinger cat states of up to 20 qubits. *Science* **365**, 574–577 (2019).
- You, J. Q. & Nori, F. Atomic physics and quantum optics using superconducting circuits. *Nature* **474**, 589–597 (2011).
- Devoret, M. H. & Schoelkopf, R. J. Superconducting circuits for quantum information: an outlook. *Science* **339**, 1169–1174 (2013).
- Martini, J. M. Qubit metrology for building a fault-tolerant quantum computer. *npj Quantum Inf.* **1**, R2493 (2015).
- Wendin, G. Quantum information processing with superconducting circuits: a review. *Rep. Prog. Phys.* **80**, 1–50 (2017).

- Preskill, J. Quantum computing in the NISQ era and beyond. *Quantum* **2**, 79 (2018).
- Brecht, T. et al. Multilayer microwave integrated quantum circuits for scalable quantum computing. *npj Quantum Inf.* **2**, 16002 (2016).
- Stassi, R. & Nori, F. Long-lasting quantum memories: extending the coherence time of superconducting artificial atoms in the ultrastrong-coupling regime. *Phys. Rev. A* **97**, 033823 (2018).
- Gu, X., Kockum, A. F., Miranowicz, A., Liu, Y.-x & Nori, F. Microwave photonics with superconducting quantum circuits. *Phys. Rep.* **718**, 1–102 (2017).
- You, J. Q., Hu, X., Ashhab, S. & Nori, F. Low-decoherence flux qubit. *Phys. Rev. B* **75**, 140515 (2007).
- Steffen, M. et al. High-coherence hybrid superconducting qubit. *Phys. Rev. Lett.* **105**, 100502 (2010).
- Yan, F. et al. The flux qubit revisited to enhance coherence and reproducibility. *Nat. Commun.* **7**, 12964 (2016).
- Córcoles, A. D. et al. Protecting superconducting qubits from radiation. *Appl. Phys. Lett.* **99**, 181906 (2011).
- Bourassa, J. et al. Ultrastrong coupling regime of cavity QED with phase-biased flux qubits. *Phys. Rev. A* **80**, 032109–8 (2009).
- Niemczyk, T. et al. Circuit quantum electrodynamics in the ultrastrong-coupling regime. *Nat. Phys.* **6**, 772–776 (2010).
- Yoshihara, F. et al. Superconducting qubit-oscillator circuit beyond the ultrastrong-coupling regime. *Nat. Phys.* **13**, 44–47 (2016).
- Forn-Díaz, P. et al. Ultrastrong coupling of a single artificial atom to an electromagnetic continuum in the nonperturbative regime. *Nat. Phys.* **13**, 39–43 (2016).
- Chen, Z. et al. Single-photon-driven high-order sideband transitions in an ultrastrongly coupled circuit-quantum-electrodynamics system. *Phys. Rev. A* **96**, 012325 (2017).
- Di Stefano, O. et al. Resolution of gauge ambiguities in ultrastrong-coupling cavity quantum electrodynamics. *Nat. Phys.* **15**, 803–808 (2019).
- Kockum, A. F., Miranowicz, A., De Liberato, S., Savasta, S. & Nori, F. Ultrastrong coupling between light and matter. *Nat. Rev. Phys.* **1**, 19–40 (2019).
- Forn-Díaz, P., Lamata, L., Rico, E., Kono, J. & Solano, E. Ultrastrong coupling regimes of light-matter interaction. *Rev. Mod. Phys.* **91**, 025005 (2019).
- Beaudoin, F., Gambetta, J. M. & Blais, A. Dissipation and ultrastrong coupling in circuit qed. *Phys. Rev. A* **84**, 043832 (2011).
- Rigetti, C. et al. Superconducting qubit in a waveguide cavity with a coherence time approaching 0.1 ms. *Phys. Rev. B* **86**, 100506–100505 (2012).
- Poyatos, J., Cirac, J. I. & Zoller, P. Complete characterization of a quantum process: the two-bit quantum gate. *Phys. Rev. Lett.* **78**, 390 (1997).
- Emerson, J., Alicki, R. & Życzkowski, K. Scalable noise estimation with random unitary operators. *J. Opt. B: Quantum Semiclass. Opt.* **7**, S347 (2005).
- Krantz, P. et al. A quantum engineer's guide to superconducting qubits. *Appl. Phys. Rev.* **6**, 021318 (2019).
- Kyaw, T. H., Allende, S., Kwek, L.-C. & Romero, G. Parity-preserving light-matter system mediates effective two-body interactions. *Quantum Sci. Technol.* **2**, 025007 (2017).
- Garziano, L. et al. One photon can simultaneously excite two or more atoms. *Phys. Rev. Lett.* **117**, 043601 (2016).
- Stassi, R. et al. Quantum nonlinear optics without photons. *Phys. Rev. A* **96**, 023818 (2017).
- Kockum, A. F., Miranowicz, A., Macri, V., Savasta, S. & Nori, F. Deterministic quantum nonlinear optics with single atoms and virtual photons. *Phys. Rev. A* **95**, 063849 (2017).
- Liu, Y.-X. et al. Optical selection rules and phase-dependent adiabatic state control in a superconducting quantum circuit. *Phys. Rev. Lett.* **95**, 087001–4 (2005).
- Baust, A. et al. Ultrastrong coupling in two-resonator circuit QED. *Phys. Rev. B* **93**, 214501–8 (2016).

## ACKNOWLEDGEMENTS

We thank K. Inomata and R.S. Deacon for useful discussions and informations. F.N. is supported in part by: NTT Research, Army Research Office (ARO) (Grant No. W911NF-18-1-0358), Japan Science and Technology Agency (JST) (via Q-LEAP and the CREST Grant No. JPMJCR1676), Japan Society for the Promotion of Science (JSPS) (via the KAKENHI Grant No. JP20H00134 and the JSPS-RFBR Grant No. JPJSBP120194828), and the Grant No. FQXi-IAF19-06 from the Foundational Questions Institute Fund (FQXi), a donor advised fund of the Silicon Valley Community Foundation. M.C. acknowledges support from NSF No. U1930403.

## AUTHOR CONTRIBUTIONS

All the authors contributed equally to this work.

## COMPETING INTERESTS

The authors declare no competing interests.

## ADDITIONAL INFORMATION

**Correspondence** and requests for materials should be addressed to R.S.

**Reprints and permission information** is available at <http://www.nature.com/reprints>

**Publisher's note** Springer Nature remains neutral with regard to jurisdictional claims in published maps and institutional affiliations.



**Open Access** This article is licensed under a Creative Commons Attribution 4.0 International License, which permits use, sharing, adaptation, distribution and reproduction in any medium or format, as long as you give appropriate credit to the original author(s) and the source, provide a link to the Creative Commons license, and indicate if changes were made. The images or other third party material in this article are included in the article's Creative Commons license, unless indicated otherwise in a credit line to the material. If material is not included in the article's Creative Commons license and your intended use is not permitted by statutory regulation or exceeds the permitted use, you will need to obtain permission directly from the copyright holder. To view a copy of this license, visit <http://creativecommons.org/licenses/by/4.0/>.

© The Author(s) 2020